TJES
ISSN: 1813-162X
Tikrit Journal of Engineering Sciences
available online at: http://www.tj-es.com

Analysis of Brushless DC Motor with Trapezoidal Back EMF with Matlab

Taha Hussain
Electrical Engineering Department, College of Engineering, University of Baghdad

(Received 05 June 2014, Accepted 10 September 2014, Available online 01 April 2015)

ABSTRACT
The dynamic characteristics such as speed and torque as well as voltages and currents of pwm brushless DC motor inverter are analyzed with a MATLAB model. The contribution of external load torque and friction torque is monitored. The switching function technique is adopted for the current control of the embedded three phase inverter that drives the brushless DC motor. In switching functions the power conversions circuits can be modeled according to their functions rather than circuit topologies. Therefore, it can achieve simplification of the overall power conversion functions. The trapezoidal type (back emf) is used in the model as it has lower switching loss compared with sinusoidal type (back emf). Results show reliable time analysis for speed, torque, phase and line voltages and currents and the effect of current commutation is clearly observed.

Keywords: BLDC motor, brushless DC motors, pwm inverter, DC motor control, trapezoidal back emf, ripple torque in brushless DC motor.

Introduction

A three-phase brushless dc motor (BLDCM) consists of permanent magnet and excitation windings. Figure 1 shows a particular type of BLDCM with a 12 poles rotor and nine slots rotor. A three phase inverter is used to supply the stator as shown in Fig.(2). The stator and rotor fields are designed to be perpendicular in order to create maximum torque. This feature is achieved by proper commutation of inverter, which acts as a commutator and brush of conventional DC motors [1]. BLDCM has high dynamic response compared with brushed DC motors. Also it has better speed versus torque characteristics, noiseless operation and high operating ranges. BLDCM are widely used in most industrial automation equipment such as robotics, medical, aerospace and so on. Simulation models of BLDCM are based in most cases on state space equations, Fourier analysis, and the d-q axis [2]. BLDCM can be classified as of sinusoidal or trapezoidal type according to the rotational voltage (back emf) induced. Trapezoidal excitation has lower switching loss while sinusoidal excitation has lower copper loss. The relatively low switching loss for trapezoidal excitation is due to the fact that only one phase is chopping at a frequency at a time while in sinusoidal type all three phase are chopping at same time. In trapezoidal commutation there will be higher torque ripple and poor harmonic performance compared with almost no torque ripple and better harmonic performance in sinusoidal commutation [3].

Modeling and simulation of BLDCM drive system

Fig.3 shows an equivalent circuit diagram for the BLDCM. The pwm inverter topology is a six-switch voltage-source with dc-link (Vd). Each phase of the three phases in BLDCM consists of a resistance, inductance, mutual inductance and back EMF [4].

STIG and inlet air spray cooling system are engaged with regenerating gas turbine cycle to increase its efficiency. Enhancement of power generation is a result of these two retrofitting methods. This further helps in developing the economy as well, as economy is directly proportional to the working of industries [8, 10]. Therefore, proper implementation of these

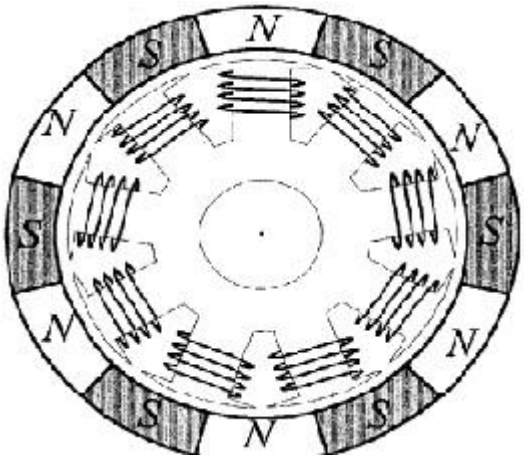

Fig.1 A 12 poles BLDCM

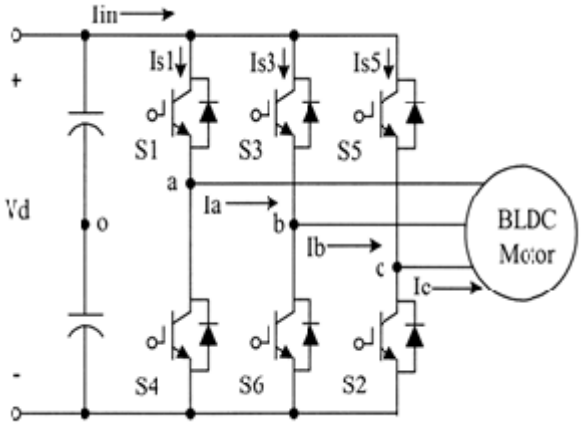

Fig. 2 A three phase inverter

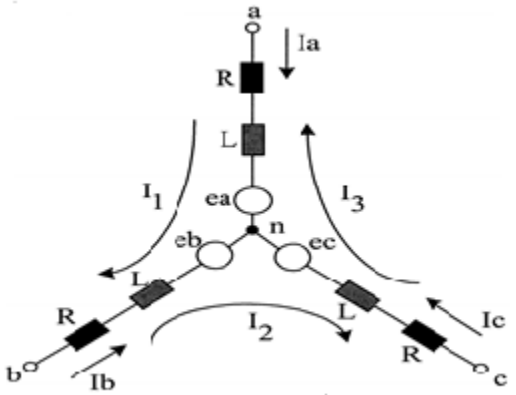

Fig.3 BLDCM equivalent circuit

The dynamic equations of BLDCM are derived as follows:

$$\left\{V_{ab} = R_{LL} i_1 + (L-M)_{LL} \frac{di_1}{dt} + e_{ab}\right\} \ldots\ldots\ldots (1)$$

$$\left\{V_{bc} = R_{LL} i_2 + (L-M)_{LL} \frac{di_2}{dt} + e_{bc}\right\} \ldots\ldots\ldots (2)$$

$$\left\{V_{ca} = R_{LL} i_3 + (L-M)_{LL} \frac{di_3}{dt} + e_{ca}\right\} \ldots\ldots\ldots (3)$$

Where V_{ab} V_{bc} , and V_{ca} are line voltages, R_{LL} is the line-to-line resistance and equals $2R$, $(L-M)_{LL}$ is the line –to-line inductance and equals to $2(L-M)$, M is mutual inductance, e_{ab} , e_{bc} , and e_{ca} are the line-to-line trapezoidal back EMF's. The electromagnetic torque equation is expressed as:

$$T_e = T_L + J\frac{dw_r}{dt} + Bw_r \quad (4)$$

Where T_e is the electromagnetic torque, T_L is the load torque, J is the inertia, B is friction coefficient and w_r is the speed of BIDCM in electrical rad/s.

$$\frac{dw_r}{dt} = \frac{1}{J}(T_e - T_L - Bw_r) \quad (5)$$

$$w_r = \frac{1}{J}\int (T_e - T_L - Bw_r)dt \quad and \quad \frac{d\theta}{dt} = w_r \rightarrow \theta_r = \int w_r\, dt \quad \ldots\ldots.(6)$$

Where θ_r is the position of the rotor. The mechanical rotor speed (w_m) in rad/s is calculated as:

$$w_m = \frac{2}{p} w_r \quad \ldots\ldots\ldots\ldots(7)$$

In this work, the damping factor B is not neglected (as often in most papers) in order to find its contribution with the transient period. The three phase currents are controlled in a type of quasi-square waveform in order to be synchronized with the trapezoidal back EMF to achieve the desired constant torque.

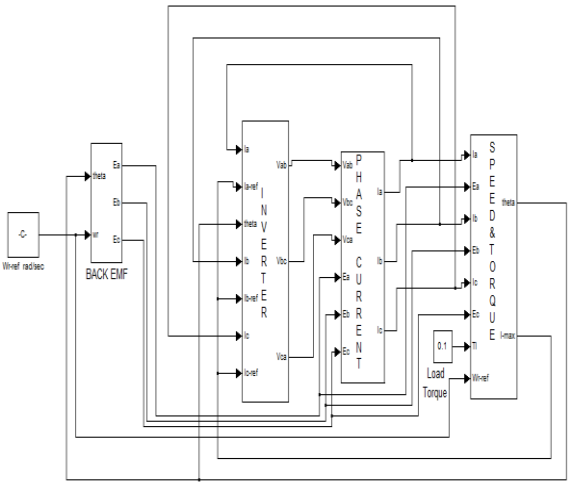

Fig.4 Overall circuit diagram for BLDCM

1.1 Modeling of trapezoidal back EMF

The back EMF is a function of rotor position θ_r and has amplitude of

$E = k_e.w_r \; where \; k_e \; is \; the \; back \; EMF \; constant$

The three phase back EMF's can be generated uniquely for every operating speed. Based on the rotor position (θ_r) and shown in Fig.5 the numerical expression of the back EMF can be obtained as in Table (1). The back EMF is implemented with a series of (IF blocks) together with (merge block) to simulate the process in Table (1) and shown in Fig.6 for phase (a).

Table 1. Generation of back Emf based on rotor position

θ_r (rotor position)	e_a (back EMF)	e_b (back EMF)	e_c (back EMF)
$0 < \theta_r < \pi/6$	$(6/\pi).\theta_r$	-1	1
$\pi/6 < \theta_r < \pi/2$	1	-1	$-(6/\pi).\theta_r + 2$
$\pi/2 < \theta_r < 5\pi/6$	1	$(6/\pi).\theta_r - 4$	-1
$5\pi/6 < \theta_r < 7\pi/6$	$-(6/\pi).\theta_r + 6$	-1	-1
$7\pi/6 < \theta_r < 9\pi/6$	-1	1	$(6/\pi).\theta_r - 8$
$9\pi/6 < \theta_r < 11\pi/6$	-1	$-(6/\pi).\theta_r + 10$	1
$11\pi/6 < \theta_r < 2\pi$	$(6/\pi).\theta_r - 12$	-1	1

System Description

Figure 1 shows a regenerative cycle two-shaft gas turbine system. It primarily consists of compressor, combustor, gas turbine and a generator. The system shown in the figure is incorporated with both injection gas turbine and inlet air cooling. It is also installed with an evaporative fog cooling system (FCS) to reduce the temperature of ambient air to state

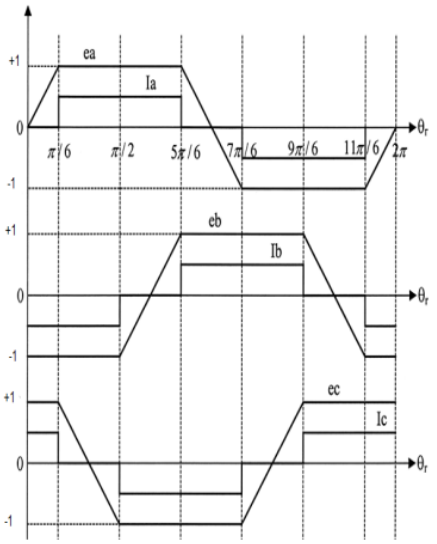

Fig.5 Generation of back emf based on rotor position

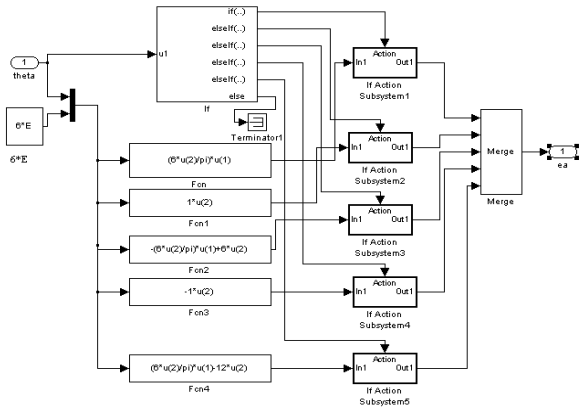

Fig.6 Implementation of back emf for phase (a)

1.2 Speed and torque control block

The electromagnetic torque is composed of $(T_e = T_a + T_b + T_c)$ where T_a , T_b *and* T_c are the torques developed by phases a, b and c respectively. The load torque is subtracted from the electromagnetic torque to get the net torque which drives the BLDCM. The torque and speed control circuit can be implemented according to equations (4,5,6 and 7) as shown in Fig.7.The output node(2) in Fig.7 refers to reference current I-max which is compared with actual load current to produce the switching functions. The function of the PI controller is to tune I-max to optimum value that matches the transient period. The friction (B damping effect) is inserted as negative feedback coefficient at the inputs of torque box.

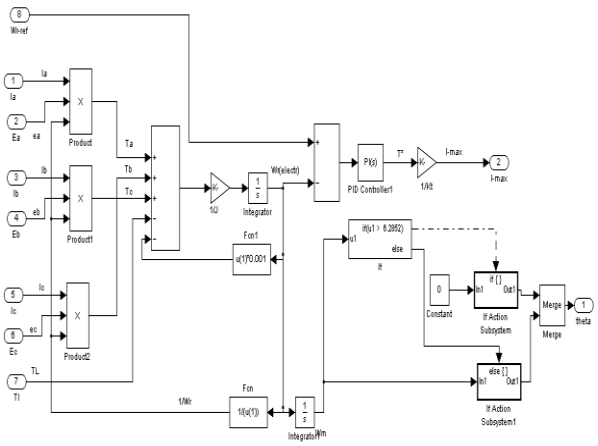

Fig.7 Implementation of speed and torque including friction torque

1.3 Dynamic response during transient analysis

The current control for phases a, b, and c can be divided into different periods following the polarity of the current. A reference current is needed to find the exact period of the actual current. An upper limit (UL) of (1.05*reference current) and a lower limit (LL) of (0.95*reference current) are used to find out which switch must be on or off in the inverter model. The actual current (load current) may have increasing or decreasing slops associated with upper and lower limits as shown in Fig.8. A memory block which stores the previous value of its input is used to simulate this differentiation process (i.e. I'_a). Table (2) shows possible switch states results from the comparison between the load current and the reference current. These switching actions are used to control the inverter model.
Table (2) switch states defined by lower and upper limits of I_{max} compared with load current and the reference current. These switching actions are used to control the inverter model.

Table 2. switch states defined by lower and upper limits of I_{max} compared with load current

$Ia > 0$	$Ia < LL$	$I_a > UL$	$LL < I_a < UL$ & $I'_a < 0$	
	S_1 on	S_1 off D_4 on	S_1 On	S_1 off D_4 on
$Ia < 0$	$I_a > UL$	$Ia <$LL	$LL < I_a < UL$ & $I'_a > 0$	
	S_4 On	S_4 off D_1 on	S_4	S_4 off D_1 on

1.4 Switching functions Following Table 2 the switching function SF_a is derived to control the current in phase a in the pwm inverter system. Other switching functions SF_b and SF_c are determined via comparing phases currents I_b and I_c with their respective reference currents. In switching functions the power conversions circuits can be modeled according to their functions rather than circuit topologies [10]. Therefore, it can achieve simplification of the overall power conversion functions. The detailed switching function of phase (a) is shown in Fig.9.

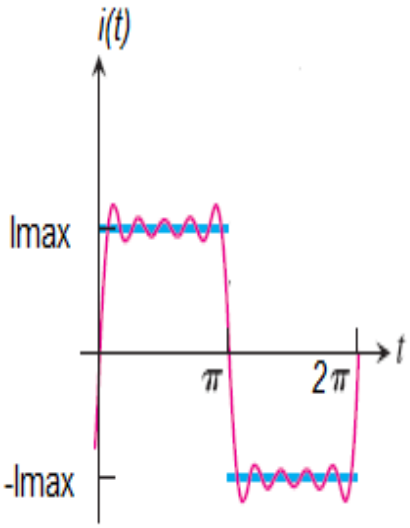

Fig.8 Reference and load current

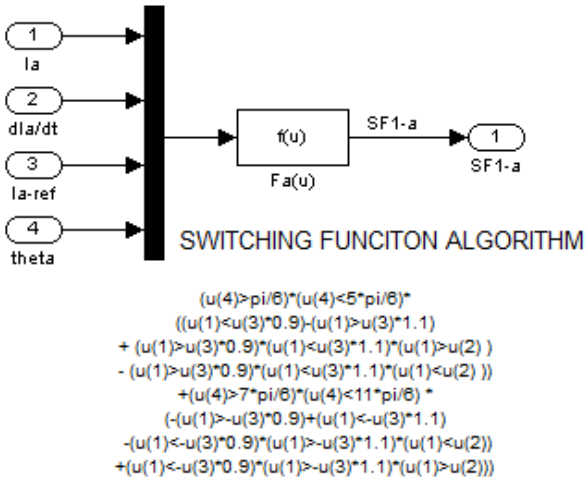

Fig.9 Implementation of the switching function of phase (a)

1.5 Simulink block for the three phase inverter drive

From equations (1, 2, and 3) together with switching functions the model for the inverter drive is shown in Fig. 10. Phase currents can be determined from line currents as follows:

$$i_a = i_1 - i_3\ ,\ i_b = i_2 - i_1,\ i_c = i_3 - i_2 \quad \ldots\ldots (8)$$

Then the inverter line-to-line voltage can be derived as:

$$v_{ab} = v_{a0} - v_{b0} = \frac{v_d}{2}(SF_a - SF_b) \ldots\ldots\ldots\ldots (9)$$

$$v_{bc} = v_{b0} - v_{c0} = \frac{v_d}{2}(SF_b - SF_c) \ldots\ldots\ldots\ldots (10)$$

$$v_{ca} = v_{c0} - v_{a0} = \frac{v_d}{2}(SF_c - SF_a) \ldots\ldots\ldots\ldots (11)$$

All values of currents and voltages, (i.e. rms, average etc.) can be calculated and manipulated easily in Matlab workspace.

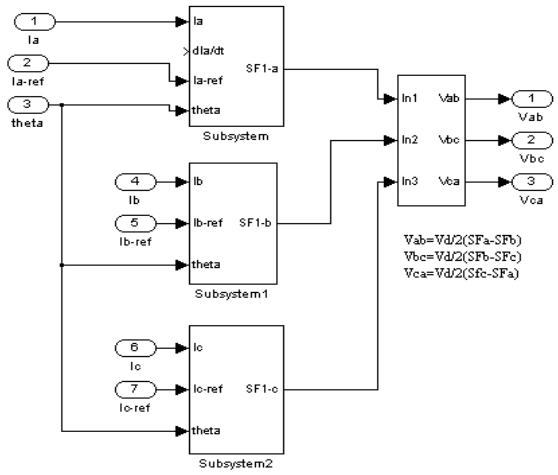

Fig.10 Implementation of the three phase inverter drive

Simulation results

The specification of the adopted BLDCM include: K_t=0.21476 N.m, $K_{e\text{-}LL}$=0.21486 V/(rad/s), J=8.2614e-5 kg.m^2, T_L=0.662 N.m, R_{LL}=1.5Ω, $(L\text{-}M)_{LL}$=6.1mH and rated mechanical speed ω_m=2500 rpm[5] are used for the simulation in Matlab. The three phase symmetric back EMF wave forms are generated according to table (1) for phase and line voltages. Figs (11-a) shows back emf's for phases a,b, and c with reference to rotor position which is varied from $0\ to\ 2\pi$ per electric cycle . The corresponding back emf's for line voltages is shown in Fig.(11-b). For 2500 rpm the electric cycle is calculated as: $\omega_e = \omega_m(P/2)$, where ω_e is the electrical speed and P=2 is the number of pair of poles. A simple calculation determines ω_e=41.66 cycles/sec and the period of one cycle is T=1/41.66=0.024 sec.

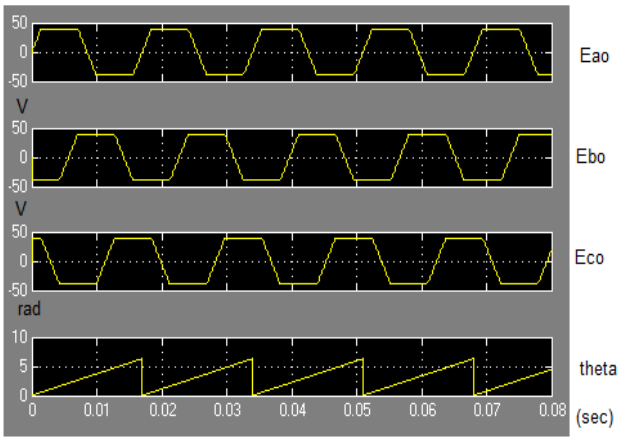

Fig.11 a- back emf's with reference to rotor

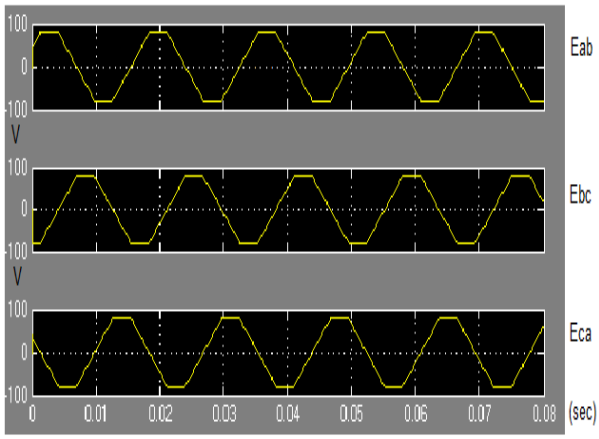

b- Line back emf's

Fig.12-a shows the phase currents I_a, I_b and I_c. The commutation takes place every 120° conduction period. This pulsating ripple is shown in Fig. (12-b) for the line currents I_1, I_2, and I_3.

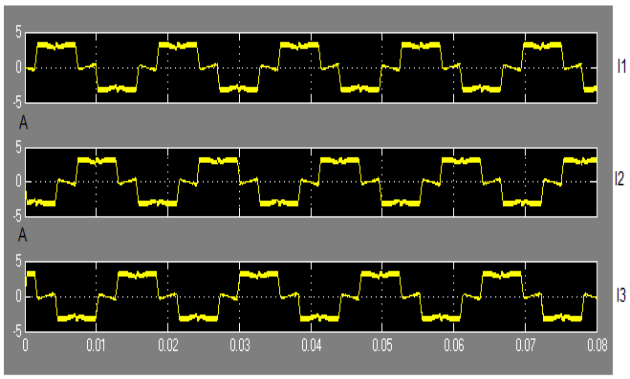

Fig.12 a- phase currents

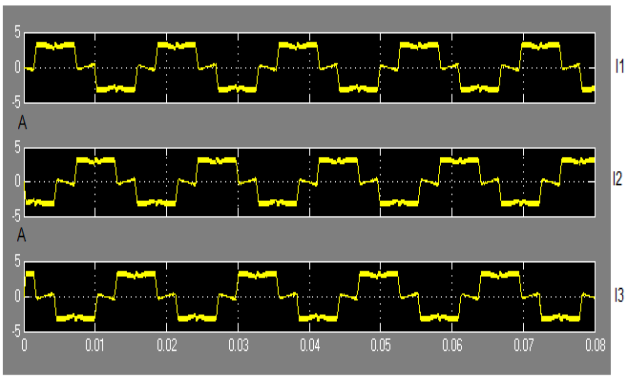

b- Line currents

The dynamic response of the speed and the shaft torque (with $T_L = 0$) are shown in Figs (13-a and 14-a) respectively. The actual speed follows the desired speed in less than 0.02s as a result of efficient tuning of the PI controller for both the integral and proportional coefficients. When external load torque of $T_L = 0.1\ N.m$ for example is added then the system reaches its steady state in more than 0.02s as shown in Fig. (13-b and 14-b).

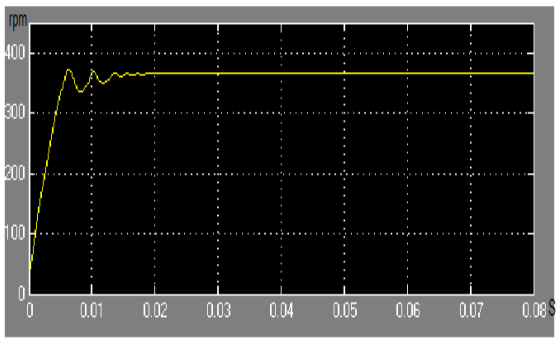

Fig.13 a- Speed at no load torque

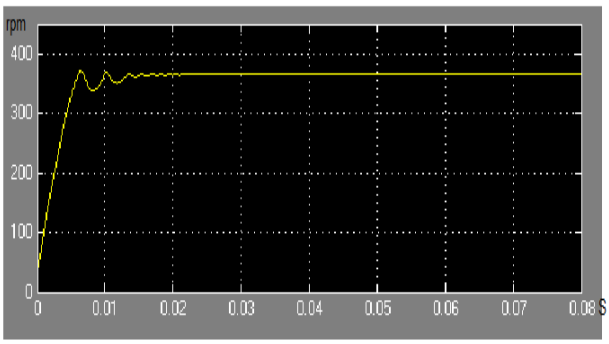

b- Speed with load torque T_L = 0.1 N.m

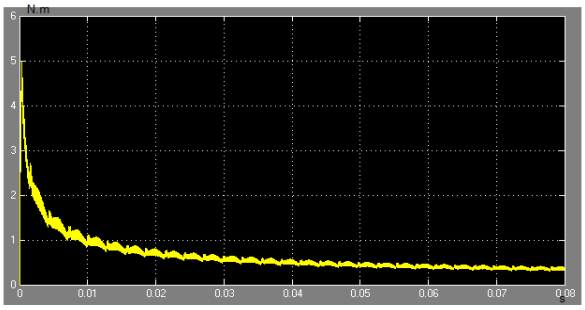

b- Shaft torque at Tl=0.1 N.m

The switching functions are shown in figure (15-a). These functions are generated during the 120^0conduction periods in order to allow the currents to be switched between the upper and lower bands. Fig.15-b shows the expanded version of switching function. The positive value (1) represents the upper band and the negative value (-1) represents the lower band.

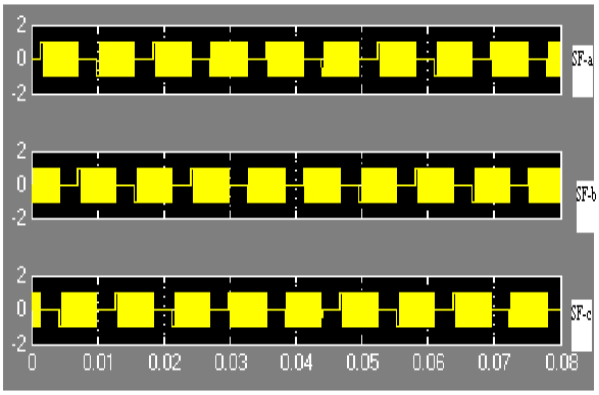

Fig.15a- Switching functions a, b and c

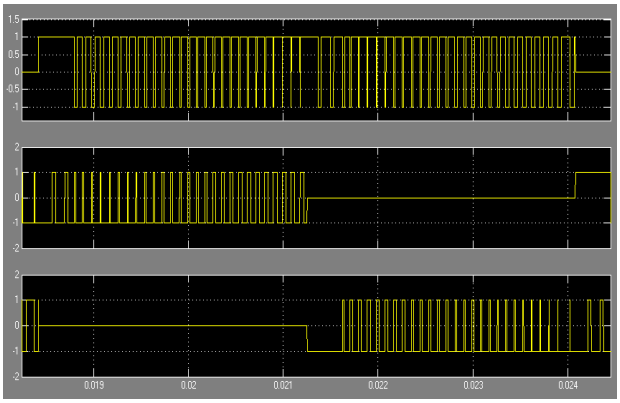

b- Expanded switching function of phase a

The phase voltages and line to line voltage are shown in Fig. 16-a and 16-b respectively.

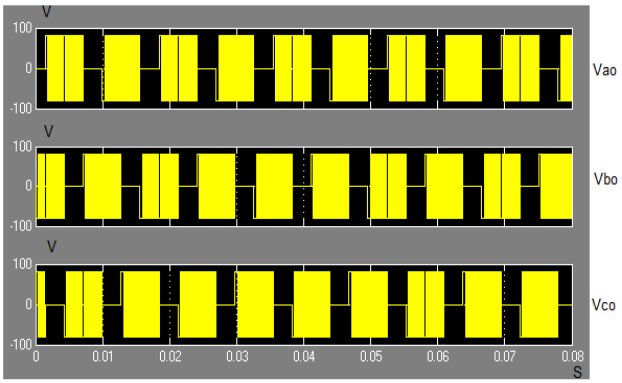

Fig. 16 a- Phase voltages

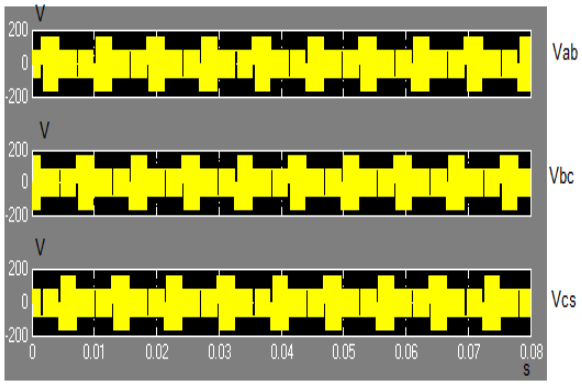

b- Line voltages

Other values such as the diode, transistor voltages and currents can be obtained easily and analyzed to see their characteristics during switching modes. Also, the external load torque can be varied and monitored to see its effect on the actual speed and to test the efficiency of the control blocks in order to quickly reach the desired speed.

Conclusion

The analysis of the dynamic as well as the electrical characteristics of the BLDCM has been analyzed with the aid of Matlab environment. The BLDCM model adopted in this work is accounts the effect of friction torque and a reliable model for switching functions have been added. Results in time domain for torque, speed, back emf, phase and line voltages and currents and the effect of external load torque have been monitored and analyzed. Any abnormal conditions can be loaded and analyzed without change in the model. The hardware implementation of this work could be implemented with recent development of the available DSP kits, of them TMS320F2812.

References

1. J. R. Hendershot and T. J. E. Miller, Design of Brushless Permanent-Magnet Motor, Oxford: Oxford Science, 1994.
2. J. P. Johnson and M. Ehsani, “Review of sensorless methods for brushless DC,” Proc. of the IEEE Industry Application Society Annual Meeting IAS’99, pp. 143–150, 1999.
3. S. K. Safi, P. P. Acarnley, and A. G. Jack, “Analysis and simulation of the high-speed torque performance of brushless DC motor drives,” Proc. of the IEE, vol. 142, 1995.
4. B. K. Lee and M. Ehsani, “A simplified functional model for 3-phase voltage-source inverter using switching function concept,” IEEE Trans. on Industrial Electronics, vol. 48, no. 2, pp. 309–321, April 2001.
5. B.K. Lee and M. Ehsani, Advanced Simulation Model for Brushless DC Motor Drives, Electric Power Components and Systems ***$**, 841–868, 2003.
6. Mehmet Cunka and Omer Aydoğdu, ‘releization controller brushless dc motor drives using Matlab/Simulink’, Mathematical and Computational Applications, Vol. 15, No.2pp218229, 2010.
7. W. Hong, W. Lee, and B.K. Lee, Dynamic Simulation of Brushless DC Motor Drives Considering Phase Commutation for Automotive Applications, Electric Machines & Drives Conference, IEMDC '07, 2007.
8. J. Figueroa, C. Brocart, J. Cros, and P. Viarouge, Simplified simulation methods for Poly phase brushless DC motors, Mathematics and Computers in Simulation, 2003.
9. C.W. Hung; C.T. Lin, and C.W. Liu, An Efficient Simulation Technique for the Variable Sampling Effect of BLDC Motor Applications, IECON 2007, 2007.
10. B. K. Lee and M. Ehsani, “A simplified functional model for 3-phase voltage-source inverter using switching function concept,” IEEE Trans. on Industrial Electronics, vol. 48, no. 2, pp. 309–321, April 2001.